Transport of small and neutral solutes through reverse osmosis membranes: Role of skin layer conformation of the polyamide film

Revised manuscript submitted to

Journal of Membrane Science

December 2017

Takahiro Fujioka[1,*], Brian E. O'Rourke[2], Koji Michishio[2], Yoshinori Kobayashi[2], Nagayasu Oshima[2], Hitoshi Kodamatani[3], Takuji Shintani[4], Long D. Nghiem[5]

[1]*Water and Environmental Engineering, Graduate School of Engineering, Nagasaki University, 1-14 Bunkyo-machi, Nagasaki 852-8521, Japan*

[2]*National Metrology Institute of Japan, National Institute of Advanced Industrial Science and Technology, 1-1-1 Umezono, Tsukuba, Ibaraki 305-8568, Japan*

[3]*Division of Earth and Environmental Science, Graduate School of Science and Engineering, Kagoshima University, 1-21-35 Korimoto, Kagoshima 890-0065, Japan*

[4]*Division of Advanced Membrane Science and Technology, Graduate School of Science, Technology and Innovation, Kobe University, 1-1 Rokkodai-cho, Kobe 657-8501, Japan*

[5]*Strategic Water Infrastructure Laboratory, School of Civil Mining and Environmental Engineering, The University of Wollongong, NSW 2522, Australia*

---

* Corresponding author: Takahiro Fujioka, Email: tfujioka@nagasaki-u.ac.jp, Ph +81 095 819 2695

Abstract

The polyamide skin layer of reverse osmosis (RO) membranes was characterised using advanced and complementary analytical techniques to investigate the mechanisms underlying the permeation of contaminants of emerging concern in potable water reuse – *N*-nitrosodimethylamine (NDMA) and *N*-nitrosomethylethylamine (NMEA). This study used five RO membrane samples with similar membrane properties. The five RO membrane samples spanned over a large range of water permeance (0.9–5.8 L/m^{2}hbar) as well as permeation of NDMA (9–66%) and NMEA (3–29%). Despite these differences among the five RO membranes, characterisations of the skin layer using positron annihilation lifetime spectroscopy, atomic force microscopy and field emission scanning electron microscopy revealed almost no variation in their free-volume hole-radius (0.270–0.275 nm), effective surface area (198–212%) and thickness (30–35 nm) of the skin layer. The results suggest that there could be other RO skin layer properties, such as the interconnectivity of the protuberances within the polyamide skin layer additional to the free-volume hole-size and thickness of the skin layer, which can also govern water and solute permeation.

Keywords: free-volume hole; *N*-nitrosodimethylamine; positron annihilation lifetime spectroscopy; potable reuse; reverse osmosis.

1. Introduction

N-nitrosodimethylamine (NDMA; $C_2H_6N_2O$) and *N*-nitrosomethylethylamine (NMEA; $C_3H_8N_2O$) are micropollutants of significant concern in potable water reuse since they are probable carcinogenic chemicals [1]. With a molecular weight of 74 g/mol, NDMA is the smallest in the *N*-nitrosamine group. NDMA and NMEA are neutral and hydrophilic compounds at environmental pH (i.e. pH 6–8). Although reverse osmosis (RO) membrane separation can achieve excellent rejection of a range of impurities in reclaimed water including salts, macro-organics, and many micropollutants, the rejection of NDMA, NMEA and several other *N*-nitrosamines is low and highly variable because of its small molecular size and lack of charge [2-5]. Thus, they are often detectable in RO permeate at concentrations higher than guideline or target values set by water authorities around the world. For example, California has established a notification level of 10 ng/L for NDMA and a public health goal of 3 ng/L [6]. Similarly, in Australia, the guideline value of NDMA in water intended for potable reuse has been also set at 10 ng/L [7]. The low and highly variable separation performance of RO with respect to NDMA rejection necessitates post treatment by advanced oxidation (UV irradiation and H_2O_2) [8]. Recent research [9] suggests that NDMA rejection by RO membranes varies significantly amongst the many RO membranes available on the market. Thus, further insights which lead to better membrane selection and improvement of the separation performance of RO for *N*-nitrosamine removal can directly contribute to the economic viability and public safety of potable water reuse.

Given the significant importance of low molecular weight micropollutants in potable reuse, numerous previous studies have been conducted to reveal the permeation mechanisms of micropollutants through RO membranes [10-13]. The significance of steric (size) interaction between solutes and the free-volume holes within the RO membrane active skin layer has

been clearly demonstrated from the viewpoint of solute properties. A strong correlation between molecular size (e.g. minimum molecular width or projected area) of uncharged solutes and their removals by RO has been established [14, 15]. Nevertheless, mechanisms underlying the difference in NDMA permeation among RO membranes are still poorly understood from the perspective of membrane properties. This is mainly due to analytical limitations in characterising the membrane skin layer at sub-nanometre scale resolution.

The free-volume holes – holes in the membrane skin layer in polymeric matrix – are thought to play an important role in water and solute transport through the RO membrane. Nevertheless, findings to date remain inconclusive. The free-volume hole size can be determined by positron annihilation lifetime spectroscopy (PALS) [16]. Previous measurements of the free-volume hole-radius of commercial RO membranes [16-18] varied considerably from 0.20 and 0.29 nm. Several previous studies [18-20] have demonstrated a strong correlation between solute permeation and free-volume hole-size. In contrast, no clear correlation between solute permeation and free-volume hole-size was reported by several other studies [17, 21, 22]. To date, there have been very few PALS studies on the characterisation of RO membranes due to the limited availability of slow positron beam based instruments.

The thickness of the skin layer has also been considered as an important property of an RO membrane governing water and solute transport. According to the solution-diffusion model [23-25], permeation of solutes and solution through RO membranes occurs via their penetration into the membrane material and diffusion through the RO membrane. The key role of the polymeric membrane thickness on solute permeation can also be supported by the finding that the thickness is inversely proportional to water permeance and there is a trade-off between water permeance and solute selectivity [26, 27]. This mechanism is plausible,

however, it is difficult to validate for commercial RO membranes. Recent RO membranes are designed with a rougher membrane surface that holds a higher surface area and a higher permeance [28-32]. As a result, they commonly have a so-called “ridge-and-valley” structure and hollow interior of crumpled nodules throughout the surface of the skin layer [29]. The entire thickness of the skin layer of commercial RO membranes is about 200-300 nm as reported by previous studies using transmission electron microscopy (TEM) [33-36]. The crumpled film forming the crumpled structure of the skin layer and the flat film comprising the interface between polyamide and polysulfone layers both have a thickness as low as 20 nm [31, 37, 38]. Characterisation using a field emission - scanning electron microscope (FE-SEM) [37] allows for a quantification of each polyamide film. Nevertheless, due to the complex inner structure and rough surface morphology of the RO membrane skin layer and its variation among RO membranes, it is still difficult to identify the location of the most important polyamide films and quantify their thickness for comparison among different RO membranes.

A systematic evaluation of several RO membranes with similar chemical ingredients can potentially yield new insights into the role of the membrane skin layer on solute permeation. This study aims to identify key structure parameters that govern NDMA transport in the RO process by characterising the skin layer properties of five RO membranes that have similar chemical composition and skin layer structure. State-of-the-art analytical techniques including PALS, FE-SEM and atomic force microscopy (AFM) were used for the characterisation of the skin layer including free-volume hole-size, thickness and surface area, respectively.

2. Materials and methods

2.1. Chemicals

Analytical grade NDMA and *N*-nitrosomethylethylamine (NMEA) **(Table 1)** were purchased from Ultra Scientific (Kingstown, RI, USA). All stock solutions were prepared in methanol to obtain 1 µg/mL of each chemical and were stored at 4 °C in the dark. Both chemicals can be classified as hydrophilic and neutral (uncharged) at environmental pH (pH 6 to 8) [39].

Table 1 – Structure and properties of the selected *N*-nitrosamines.

Compound	NDMA	NMEA
Structure	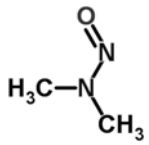	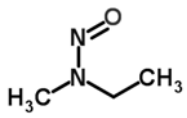
Molecular formula	$C_2H_6N_2O$	$C_3H_8N_2O$
Molecular weight [g/mol]	74.05	88.06
Log *D* at pH8[a] [-]	0.04	0.4
pKa at pH8[a] [-]	3.5	3.4
Minimum projection area[a, b] [nm^2]	0.20	0.22

[a] Chemicalize (http://www.chemicalize.org).
[b] Minimum projection area is the area of the compound projected with the minimum plane of its circular disk, based on the van der Waals radius.

2.2. Membranes and membrane treatment system

Two commercially available RO membranes – namely ESPA2 and ESPAB – and a prototype RO membrane were obtained as flat sheet samples from Hydranautics/Nitto (Osaka, Japan). The active skin layers of these membranes have similar chemical ingredients although the detailed information is proprietary. The ESPA2 membrane has been employed in many potable water reuse schemes [14], while the ESPAB membrane is designed for boron removal and has been widely used in the second pass of RO seawater desalination plants. In addition, samples of the ESPAB and Prototype membranes were also subjected to heat treatment to

alter the physical properties. These heat-treated samples are designated as heated ESPAB and heated Prototype, respectively. Thus, in total, five different membrane samples were used in this investigation.

2.3. Experimental protocols

2.3.1. Heat treatment

Heat treatment was conducted by heating the RO membrane coupons in 80 °C ultrapure water solution. The RO membrane coupons were first rinsed with ultrapure water (18.0 MΩcm). Thereafter, each coupon was stored in a 200 mL beaker filled with ultrapure water, and the beakers were placed in a temperature-controlled water bath (SWB-11A, AS ONE, Osaka, Japan) that maintained the water temperature at 80 °C. After 4 h of heat treatment, the membrane coupons were rinsed with ultrapure water and stored at 4 °C in the dark.

2.3.2. RO filtration experiments

The separation of NDMA and NMEA by each RO membrane was evaluated in ultrapure water using the bench-scale cross-flow RO system **(Fig. S1)**. Filtration experiments were started with permeance evaluation in which RO membrane filtration experiments were conducted with ultrapure water at 2000 kPa to measure the pure water permeance. Thereafter, NDMA and NMEA stock solution was added to obtain 200 ng/L of each compound in the feed solution. The membrane system was operated at a 20 L/m^{2}h permeate flux and 20 °C feed temperature. Concentrations of NDMA and NMEA were determined by high-performance liquid chromatography-photochemical reaction-chemiluminescence as described in our previous studies [40, 41]. The passage is defined as $R = 100 \times C_p/C_f$, where C_p and C_f are solute concentration in the permeate and feed, respectively.

2.4. Membrane characterisations

2.4.1. Surface chemistry

Major functional groups of RO membranes was analysed using Fourier transform infrared spectroscopy (FTIR) spectrophotometer (Nicolet iS5, Thermo Fisher Scientific, Waltham, MA, USA) in attenuated total reflection (ATR) method. The RO membrane samples were freeze-dried for 24 hours using a freeze drier (FD-1000, Tokyo Rikakikai, Tokyo, Japan). The spectrum was obtained in the range of 400-4000 cm^{-1} at 1 cm^{-1} resolution.

2.4.2. Positron annihilation lifetime spectroscopy (PALS)

The free-volume hole-radius of each RO membrane was measured using PALS with a slow positron beam that is housed at the National Institute of Advanced Industrial Science and Technology (AIST) in Tsukuba, Japan. Details of PALS for the analysis of RO membranes are provided elsewhere [9]. The radius of free-volume hole (r) of the skin layer in RO membranes was determined from the pick-off annihilation lifetime of *ortho*-positronium ($\tau_{o\text{-}Ps}$) using the Tao-Eldrup model [42, 43]:

$$\tau_{o-Ps} = 0.5\left[1 - \frac{r}{r+0.166} + \frac{1}{2\pi}\sin\left(\frac{2\pi r}{r+0.166}\right)\right]^{-1} \quad (1)$$

where r (< 1nm) is approximated as a spherical shape. Positron irradiation was carried out under vacuum (~ 10^{-5} Pa) and about 2×10^6 positron annihilation events were collected for the positron lifetime spectrum of each sample. Spectra were analysed using a non-linear least-squares fitting program. Unless otherwise stated, the incident energy (E_{in}) was set at 1.0 keV, which corresponds to a mean implantation depth of 31 nm from the top (implantation depth range = 0–90 nm) with a material density of 1.3 g/cm^3 (**Fig. 1**). This incident energy was selected according to previous studies [18, 19] that revealed the lowest free-volume hole-

radius of polyamide RO at 1.0 keV. The dry material density of RO membranes (1.3 g/cm^3) was determined based on the data reported by Kolev and Freger [44].

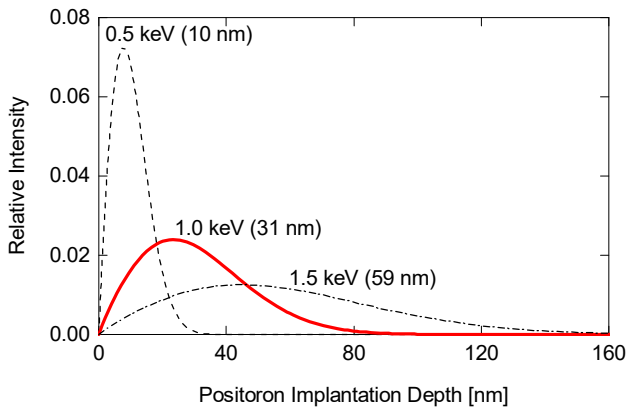

Fig. 1 – Distribution of positron implantation depth in a polyamide membrane sample with a material density of 1.3 g/cm^3 at a positron incident energy of 0.5, 1.0 or 1.5 keV. The mean implantation depth at each positron incident energy is shown in brackets.

2.4.3. Atomic force microscopic analysis

Membrane surface area was analysed using an atomic force microscope (AFM) (MFP-3D-SA, Asylum Research – Oxford Instruments Company, CA, USA). Membranes underwent sample pre-treatment steps involving the replacement of water in the membranes with tert-Butyl alcohol followed by freeze drying. Images were obtained in air using tapping mode with a silicate cantilever. The scanning area was 5 µm × 5 µm. The effective surface area of each membrane was calculated based on the data of three samples. Effective surface area here was defined as a ratio between the actual (measured) area and the sample area as described in the following formula:

$$Effecticve\ surface\ area\ [\%] = \frac{Actual\ area\ [\mu m^2]}{Sample\ area\ [\mu m^2]} \times 100 \qquad (2)$$

2.4.4. Field emission scanning electron microscopic analysis

Cross-sectional images of the RO membrane skin layer were attained using a field emission - scanning electron microscope (FE-SEM) instrument (S-4800, Hitachi, Japan) at 3 kV accelerating voltage. Cross-sections of each membrane sample were prepared by freeze-fracturing wet membranes in liquid nitrogen followed by air drying. Thereafter, the target cross-sectional area was coated with conductive material prior to the analysis. The thickness of the skin layer of each RO membrane was calculated by determining the average of 5 different locations.

3. Results and discussion

3.1. Solute permeation

The five RO membrane samples examined in this study spanned over a large range of water permeance as well as solute passage with respect to both NDMA and NEMA **(Fig. 2)**. Heat treatment was effective to reduce solute passage and water permeance. After heat treatment, NDMA passage through the ESPAB and the Prototype membranes decreased from 56 to 37% and from 18 to 9%, respectively. The pure water permeance of these membrane also proportionally decreased as can be seen from **Fig. 2**. A strong linear correlation between solute passage with respect to both NDMA and NMEA and water permeance can be confirmed in **Fig. 2**. As noted in section 2.2, all five RO membrane samples were from the same manufacturer with similar chemical ingredients of the active skin layer. Thus, data from **Fig. 2** allow for a systematic investigation of the role of the active skin layer in transport of small and neutral solutes as well as water across the membrane.

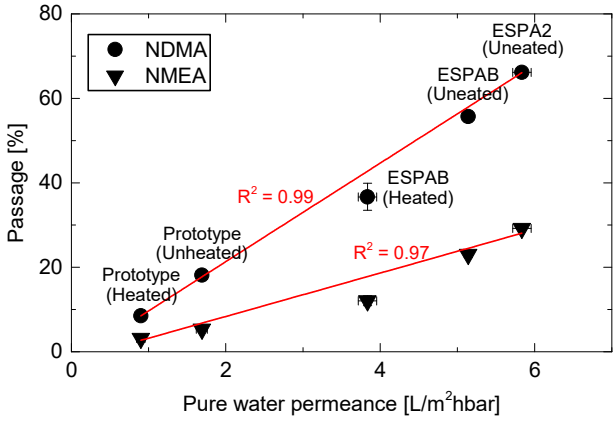

Fig. 2 – Correlation between the passage of NDMA and NMEA in pure water, and pure water permeance (feed temperature = 20.0 ± 0.1 ºC and permeate flux = 20 L/m^{2}h). Error bars show the range of two replicate experiments.

3.2. Characterisations of the RO skin layer

3.2.1. Membrane chemistry

Variation in the top layer chemistry of RO membranes can be qualitatively evaluated by examining the FTIR spectra [45, 46]. Notable peaks for fully aromatic polyamide were observed at 1668, 1608 and 1539 cm^{-1} that correspond to C=O and C-N stretching and C-C-N deformation vibration (amide I), N-H deformation vibration and C=C ring stretching vibration of aromatic amide, and N-H in-place bending and N-C stretching vibration of a -CO-NH- group (amide II), respectively [47] **(Fig. S2)**. Peaks at 1586, 1505, 1488 and 1245 cm^{-1} can be assignable to polysulfone. The ratio in peak intensity between 1668 cm^{-1} (C=O stretching of the amide group formed by the reaction between diamine and acid chloride) and 1245 cm^{-1} (C-O stretching of the polysulfone support) was 0.21, 0.21 and 0.17 for ESPA2, ESPAB and Prototype, respectively. This indicates that these RO membranes have similar chemical composition. It is noted that heat treatment increased the peak intensity ratio from 0.21 to 0.30 and from 0.17 to 0.18 for ESPAB and Prototype membrane, respectively. The cause of the changes in the peak intensity for ESPAB after heat treatment remains unclear, but it will be in the scope of our future study.

228 3.2.2. Free-volume hole-radius

229 The mean free-volume hole-radius of the selected RO membranes was determined at a mean
230 implantation depth of 31 nm using $\tau_{o\text{-Ps}}$ values (pick-off annihilation lifetime of *o*-Ps) from
231 PALS analysis **(Table S3)**. The free-volume hole-radius of the three unheated RO
232 membranes (i.e. ESPA2, ESPAB and Prototype) was almost identical, ranging from 0.270 to
233 0.275 nm **(Fig. 3)**. Heat treatment did not show any discernible impact on the free-volume
234 hole-radius. It is noteworthy that PALS analysis at other implantation depths (i.e. 10 and 59
235 nm) of the ESPAB membrane did not show any significant variation in the free-volume hole-
236 radius due to heat treatment **(Fig. S4)**. It is noted that current PALS technique cannot confirm
237 a small difference in free-volume hole-radius of RO membranes less than 0.01 nm due to the
238 inherent error in PALS and the inhomogeneity of the membrane samples. Thus, the free-
239 volume hole-radius of all five membrane samples in **Fig. 3** are considered to be similar.

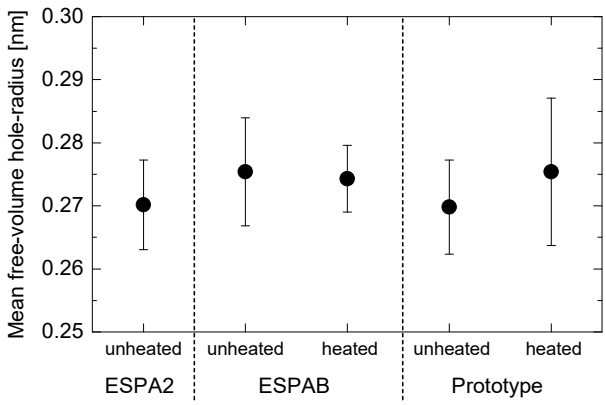

240

241 **Fig. 3** – Free-volume hole-radius of the five RO membranes. The data here is the average and
242 range of two replicates.

243 The cross-sectional areas of spherical free-volume holes with radii of 0.270 and 0.275 nm are
244 0.23 and 0.24 nm^2, respectively. These values are comparable to the minimum projection area
245 of NDMA (0.20 nm^2) and NMEA (0.22 nm^2) **(Table 1)**. Because the passage of NDMA and
246 NMEA varied with a difference of only 0.02 nm^2 in the minimum projection area of the two

247 molecules, a variation of 0.01 nm^2 in free-volume hole-area among the five RO membranes
248 may still be an important factor. However, there was no observable correlation between the
249 measured free-volume hole-radius and the passage of NDMA and NMEA **(Fig. S5)**. Given
250 the similar free-volume hole-size of the five membrane samples**,** these results suggest that a
251 factor other than the free-volume hole-size can also govern the permeation of NDMA and
252 NMEA by these RO membranes.

253 3.2.3. Effective surface area

254 The effective membrane surface area was determined by taking into account the topography
255 of the RO skin layer at the microscopic level (i.e. surface roughness) using AFM. Indeed, at
256 the microscopic level, the effective membrane surface area can differ considerably from the
257 surface area normally used to calculate the permeate flux [9]. It is noted that permeate flux
258 considerably influences NDMA permeation [13]. Since the skin layer can play an important
259 role in solute permeation through the RO membrane as proposed in literature [30, 38], it is
260 important to take into account the effective membrane surface area when assessing solute
261 permeation.

262 Despite the large variation in the visualized "ridge-and-valley" structure among the three
263 different types of RO membranes (i.e. ESPA2, ESPAB and Prototype), their effective surface
264 area was almost identical, ranging from 198 and 212% **(Fig. 4)**. In other words, the effective
265 membrane surface area at the microscopic level is approximately two times the plain area.
266 Likewise, heat treatment did not cause any discernible changes in the effective surface area.
267 Results from **Fig. 4** confirm that separation experiments in this study were also at the same
268 permeate flux for a systematic comparison of solute permeation among all selected RO
269 membranes. More importantly, the observation of the large variation in permeance **(Fig. 2)**
270 and almost identical effective surface area **(Fig. 4)** among the RO membranes suggests that in

this study, water permeance is not influenced by the effective surface area of the RO skin layer. It is noteworthy that the surface area determined by AFM does not necessarily represent the entire surface area. Surface areas through which feed solution can penetrate include the backside of bent protuberance and confined rumpled films with packed protuberances that cannot be measured by AFM [32]. Therefore, actual surface area taking account of all morphology is necessary to conclusively determine the role of surface area for water permeance.

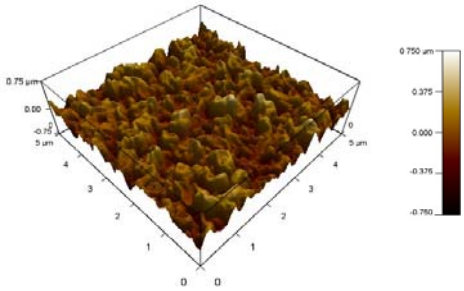

(a) ESPA2 (unheated)
Area = 212 ± 10%

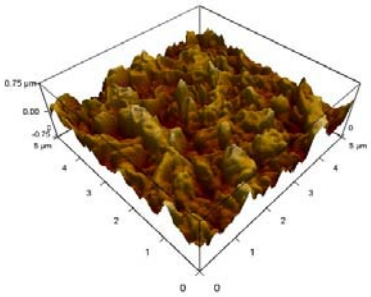

(b) ESPAB (unheated)
Area = 204 ± 6%

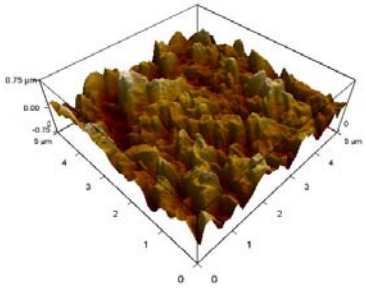

(c) ESPAB (heated)
Area = 202 ± 3%

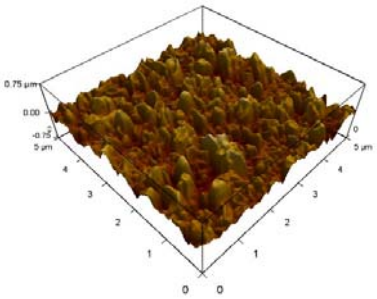

(d) Prototype (unheated)
Area = 198 ± 5%

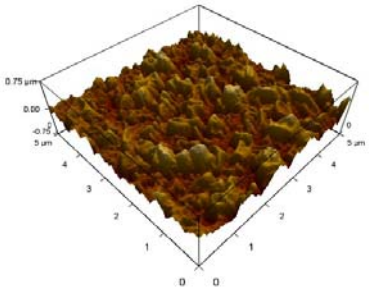

(e) Prototype (heated)
Area = 205 ± 3%

Fig. 4 – AFM images of the five RO membranes. The surface area (and error) is determined from the average (and measurement variation) of three membrane coupons.

280 3.2.4. Thickness

281 The thickness of the skin layer of the selected RO membranes was evaluated using a cross-
282 sectional view obtained by FE-SEM. The FE-SEM analysis **(Fig. 5)** revealed a distinctive
283 "ridge-and-valley" structure and a hollow interior of crumpled nodules throughout the skin
284 layer of all RO membranes investigated in this study. These complex structures are similar to
285 other commercial RO membranes recently reported in literature [36-38]. The estimated
286 thickness of the skin layer was 300-400 nm for ESPA2 and ESPAB RO membranes and 200-
287 300 nm for Prototype RO membranes. There was no apparent change in the skin layer
288 thickness after heat treatment. The skin layer of these membranes comprised of two major
289 polyamide films (A) a flat polyamide film that forms a film base at the interface with the
290 polysulfone support layer and (B) a crumpled polyamide film that forms crumpled nodules
291 with internal hollow structure (also called as protuberance) **(Fig. 5)**. Ultrahigh resolution FE-
292 SEM images in **Fig. 5** show a similar thickness between the flat polyamide film and crumpled
293 polyamide film. In addition, it appears that the crumpled polyamide film is almost always on
294 top of the flat polyamide film. Using SEM, Yan et al. [37] also reported that the ESPA2 RO
295 membrane has a through-bore that interconnects the cavity of the protuberance and open
296 structure of the polysulfone support layer. The interconnections can also be found at the other
297 four RO membranes used in this study. The majority of the protuberances did not appear to
298 have interconnections. Although high water permeance of RO membranes (e.g. ESPA2) can
299 be associated with the number of the interconnections, it was not possible to quantify the
300 connectivity through the FE-SEM cross-sectional images.

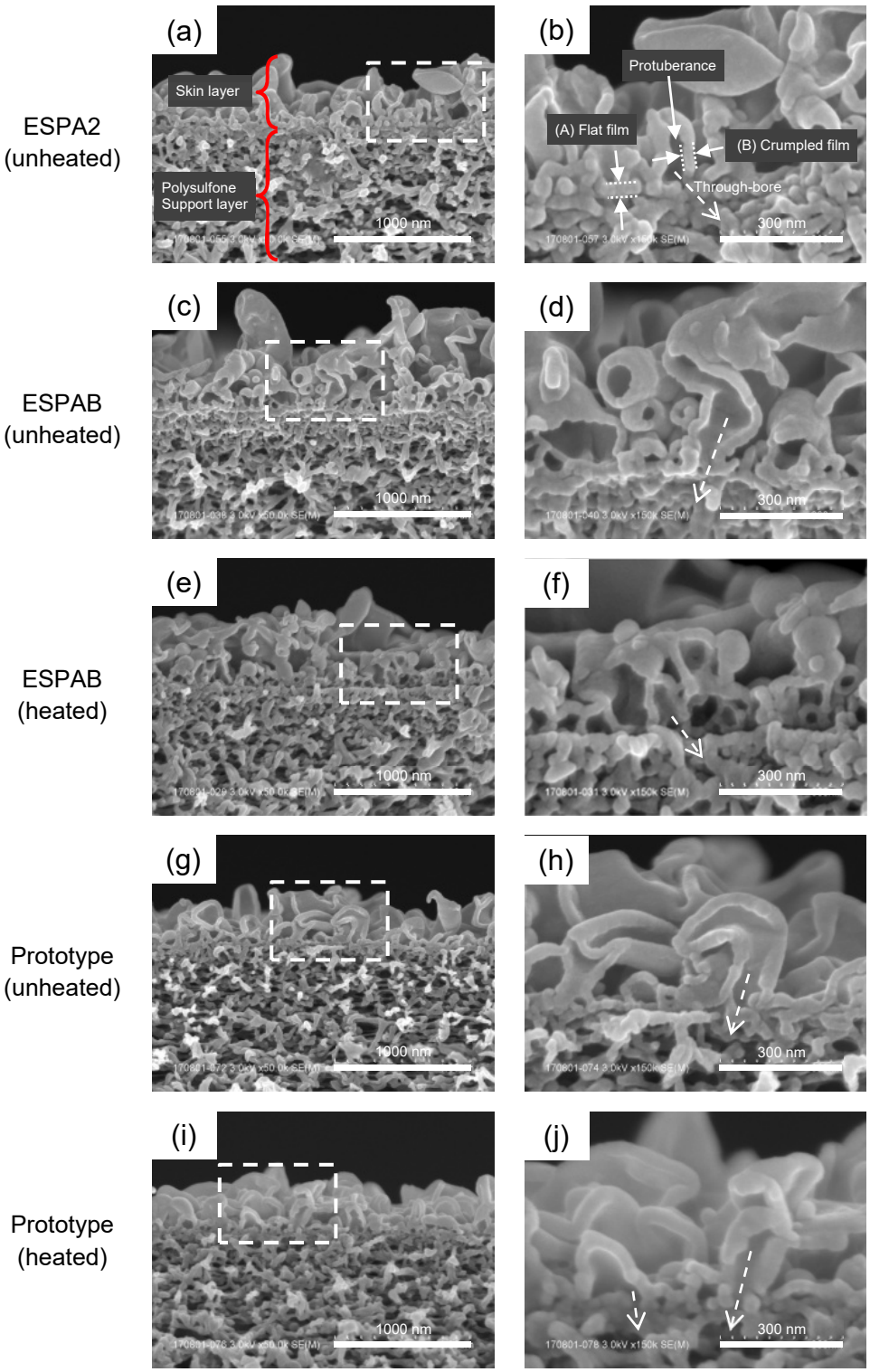

Fig. 5 – FE-SEM cross-sectional images of the five RO membranes: (a, c, e, g, i) skin & polysulfone layers (scale = 1000 nm) and (b, d, f, h, j) areas enclosed with dash lines in the skin & polysulfone layers (scale = 300 nm).

305 Given the importance of the crumpled polyamide films on water and solute permeation [30,
306 37], the crumpled film thickness was measured for all the RO membranes. It is noted that the
307 values were attained through two representative FE-SEM images; thus, there could be a
308 variation in thickness throughout the RO membranes. The results revealed that unheated
309 ESPA2, ESPAB and Prototype RO membranes had similar crumpled film thickness of 36, 29,
310 and 34 nm, respectively **(Fig. 6)**. Results in **Fig. 6** indicate that there was no discernible
311 variation in thickness among the three RO membranes in this study. In addition, heat
312 treatment did not appear to alter the crumpled film thickness. Indeed, differences in the
313 crumpled film thickness between heated and unheated samples were within the measurement
314 error margin (i.e. standard deviation of two samples of the same membrane). As a result, in
315 this study, variation in water flux and the passage of NDMA and NMEA cannot be attributed
316 to the measured crumpled film thickness **(Fig. S7)**, suggesting that other skin layer properties
317 such as conformation of the crumpled polyamide films could also govern their permeation.

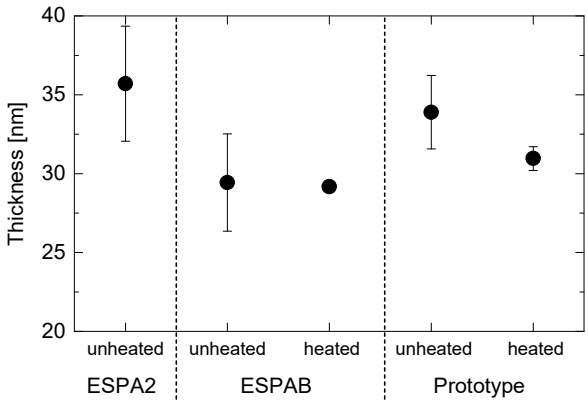

318

319 **Fig. 6** – Thickness of the crumpled film of the five RO membranes. The thickness was
320 determined based on two RO membrane coupons, each of which was measured at 5 locations
321 **(Table S6)**.

3.3. Discussions

Comprehensive analysis of the skin layer of five RO membrane samples using PALS, FE-SEM and AFM revealed that there could be other RO skin layer properties besides the free-volume hole-radius and thickness of the crumpled film that can govern water and solute permeation. This is a significant finding in membrane transport, because the free-volume hole-radius and thickness of the crumpled film have often been considered the only membrane properties governing the membrane transport.

FE-SEM images obtained here identified that the free-volume hole-radius analysed by PALS was likely to result from the crumpled polyamide film. According to the distribution of positron implantation depth **(Fig. 1)**, most positrons of PALS at a positron incident energy of 1 keV were expected to have annihilated within the crumpled polyamide films that have the thickness of about 30 nm. The flat polyamide film is mostly covered by several layers of the crumpled film and it is 300 to 400 nm away from the top ridge **(Fig. 5)**. Thus, the flat polyamide film located at the interface with the polysulfone supporting layer is not accessible by positrons with 1 keV. Although the flat polyamide film beneath the crumpled films can be reached by increasing the positron incident energy **(Fig. 1)**, increasing the incident energy also broadens out the positron implantation depth distribution, meaning that signals can be obtained from both the flat and crumpled films. As a result, thickness of the flat film that has far less surface area than the crumpled film cannot be accurately determined. If the flat polyamide film plays an important role in solute permeation, a sample preparation method that enables us to preferentially analyse the flat polyamide films should be developed.

In regard to the flat polyamide film, perhaps water permeance and separation performance of the selected RO membranes is related to the degree of the interconnections between the cavity of the protuberance and the open structure of the polysulfone support layer. In other

346 words, RO membranes with less interconnections have less water permeance but high
347 separation capability. The importance of hollow protuberance on the water permeance of RO
348 membranes has been confirmed by Pacheco et al. [48] who evaluated 3D images of two
349 commercial RO membranes using TEM tomography technique. The FE-SEM cross-sectional
350 images in **Fig. 5** revealed that not all of the protuberances have interconnections toward the
351 polysulfone support layer. Protuberances without interconnections allow the solute and
352 solvent (water) to permeate through two barriers – crumpled film and flat film, which could
353 reduce water permeance but improve the separation performance. The projected area TEM
354 technique previously reported by Pacheco et al. [36] and Yan et al. [37] has the potential to
355 visualize the structure inside the ridges including the interconnections from its top view, but
356 the correlation between the interconnections and separation performance has not yet been
357 quantified.

358 There are some other limitations and challenges for the characterization of the RO skin layer
359 with respect to PALS analysis. The analysis here was conducted under dry conditions, while
360 wet RO membranes may have swelling effects [49], which can expand the polymer network
361 and alter the water permeance and selectivity [50, 51]. In addition, the size distribution of
362 free-volume holes may be more important than mean free-volume hole-radius, because the
363 narrower passages connecting the major free-volume holes could actually determine solute
364 permeations as suggested by Dražević et al. [52]. More accurate analysis with wet membrane
365 samples and the determination of size distribution of free-volume holes requires a significant
366 improvement in PALS method, thus, it is a scope of our future study.

367 In addition to the swelling effects, chemical properties of the internal skin layer could be a
368 major contributor to a variation in diffusion coefficient and sorption coefficient of water and
369 solutes, which ultimately leads to a variation in their water permeance and separation

370 performance. Typically, increases in the degree of polyamide cross-linking can cause less
371 water and solutes to sorb onto the polymer due to restriction in swelling effects [53]. This
372 could cause a decrease in both effective water and salt diffusion coefficients [54], leading to a
373 decrease in water permeance but an increase in selectivity (D_w/D_s) (trade-off theory) [26]. If
374 that is the case, chemical properties of the skin layer such as cross-linking levels should be
375 more important than the physical properties analysed in this study (i.e. free-volume hole-
376 radius and thickness) to determine the major skin layer properties.

377 **4. Conclusions**

378 This study shows that RO membranes with distinct separation performance and water
379 permeance can have similar crumpled film properties including free-volume hole-size and
380 thickness. PALS, AFM and FE-SEM revealed that major crumpled polyamide film properties
381 such as free-volume hole-size, effective surface area and thickness are almost identical
382 among three different types of unheated RO (ESPA2, ESPAB and Prototype) and two heated
383 RO (ESPAB and Prototype). The results suggest that there exist at least another RO skin
384 layer property other than the free-volume hole-size and thickness that can also govern the
385 transport of water and small and neutral solutes such as NDMA and NMEA that are of
386 signifincant concern in potable water reuse. Such property is likely to be the protuberance
387 conformation or interconnectivity of the protuberance within the membrane polyamide skin
388 layer. In addition, FE-SEM data also reveal that current PALS technique may not be suitable
389 for determining free-volume hole-radius of the flat polyamide film located at the interface
390 between the polyamide skin and the polysulfone supporting layer beneath the crumpled
391 polyamide films. Further advances in analytical technique that allows for the quantification of
392 interconnections between the protuberances and the polysulfone support layer, the
393 comprehensive characterisation of RO membranes by PALS (size distribution and wet

conditions), and the evaluation of chemical properties of the polyamide films is necessary to fully decode the permeation mechanism of NDMA.

5. Acknowledgements

This work was supported by KWEF Research Grant Program; JSPS KAKENHI Grant Number JP16H06104; and AIST Nanocharacterization Facility (ANCF) platform as a program of "Nanotechnology Platform" of the Ministry of Education, Culture, Sports, Science and Technology (MEXT), Japan. We also thank Hydranautics/Nitto for providing RO membrane samples for this investigation.

6. References

[1] US Environmental Protection Agency, Integrated Risk Information System (IRIS), N-nitrosodimethylamine. Office of Research and Development (ORD), National Center for Environmental Assessment (1987) www.epa.gov/iris/subst/0045.htm, in, 1987.

[2] M.J. Farré, K. Döderer, L. Hearn, Y. Poussade, J. Keller, W. Gernjak, Understanding the operational parameters affecting NDMA formation at Advanced Water Treatment Plants, J. Hazard. Mater., 185 (2011) 1575-1581.

[3] C. Bellona, J.E. Drewes, G. Oelker, J. Luna, G. Filteau, G. Amy, Comparing nanofiltration and reverse osmosis for drinking water augmentation, Journal AWWA, 100 (2008) 102-116.

[4] T. Fujioka, S.J. Khan, J.A. McDonald, A. Roux, Y. Poussade, J.E. Drewes, L.D. Nghiem, *N*-nitrosamine rejection by reverse osmosis membranes: A full-scale study, Water Res., 47 (2013) 6141-6148.

[5] M.H. Plumlee, M. López-Mesas, A. Heidlberger, K.P. Ishida, M. Reinhard, N-nitrosodimethylamine (NDMA) removal by reverse osmosis and UV treatment and analysis via LC-MS/MS, Water Res., 42 (2008) 347-355.

[6] CDPH, NDMA and other Nitrosamines - Drinking water issues, California Department of Public Health 2011.

[7] NRMMC, EPHC, AHMC, Australian guidelines for water recycling: Managing health and environmental risks (Phase 2): Augmentation of drinking water supplies, Environment Protection and Heritage Council, National Health and Medical Research Council, Natural Resource Management Ministerial Council, Canberra, 2008.

[8] H.L. Leverenz, G. Tchobanoglous, T. Asano, Direct potable reuse: A future imperative, Journal of Water Reuse and Desalination, 1 (2011) 2-10.

[9] T. Fujioka, N. Oshima, R. Suzuki, W.E. Price, L.D. Nghiem, Probing the internal structure of reverse osmosis membranes by positron annihilation lifetime spectroscopy: Gaining more insight into the transport of water and small solutes, J. Membr. Sci., 486 (2015) 106-118.

[10] A.R.D. Verliefde, S.G.J. Heijman, E.R. Cornelissen, G.L. Amy, B. Van der Bruggen, J.C. van Dijk, Rejection of trace organic pollutants with high pressure membranes (NF/RO), Environ. Prog., 27 (2008) 180-188.

[11] C. Bellona, J.E. Drewes, P. Xu, G. Amy, Factors affecting the rejection of organic solutes during NF/RO treatment - A literature review, Water Res., 38 (2004) 2795-2809.

[12] L.D. Nghiem, P.J. Coleman, NF/RO filtration of the hydrophobic ionogenic compound triclosan: Transport mechanisms and the influence of membrane fouling, Sep. Purif. Technol., 62 (2008) 709-716.

[13] T. Fujioka, L.D. Nghiem, S.J. Khan, J.A. McDonald, Y. Poussade, J.E. Drewes, Effects of feed solution characteristics on the rejection of *N*-nitrosamines by reverse osmosis membranes, J. Membr. Sci., 409–410 (2012) 66-74.

[14] T. Fujioka, S.J. Khan, Y. Poussade, J.E. Drewes, L.D. Nghiem, *N*-nitrosamine removal by reverse osmosis for indirect potable water reuse – A critical review based on observations from laboratory-, pilot- and full-scale studies, Sep. Purif. Technol., 98 (2012) 503-515.

[15] Y. Kiso, K. Muroshige, T. Oguchi, M. Hirose, T. Ohara, T. Shintani, Pore radius estimation based on organic solute molecular shape and effects of pressure on pore radius for a reverse osmosis membrane, J. Membr. Sci., 369 (2011) 290-298.

[16] S.H. Kim, S.-Y. Kwak, T. Suzuki, Positron annihilation spectroscopic evidence to demonstrate the flux-enhancement mechanism in morphology-controlled thin-film-composite (TFC) membrane, Environ. Sci. Technol., 39 (2005) 1764-1770.

[17] T. Fujioka, N. Oshima, R. Suzuki, S.J. Khan, A. Roux, Y. Poussade, J.E. Drewes, L.D. Nghiem, Rejection of small and uncharged chemicals of emerging concern by reverse osmosis membranes: The role of free volume space within the active skin layer, Sep. Purif. Technol., 116 (2013) 426-432.

[18] Z. Chen, K. Ito, H. Yanagishita, N. Oshima, R. Suzuki, Y. Kobayashi, Correlation study between free-volume holes and molecular separations of composite membranes for reverse osmosis processes by means of variable-energy positron annihilation techniques, J. Phys. Chem. C, 115 (2011) 18055-18060.

[19] K. Ito, Z. Chen, W. Zhou, N. Oshima, H. Yanagishita, R. Suzuki, Y. Kobayashi, Subnanoscopic holes in composite membranes for desalination elucidated by energy-tunable positron annihilation, Jpn. J. Poly. Sci. Technol., 69 (2012) 443-447.

[20] M. Henmi, Y. Fusaoka, H. Tomioka, M. Kurihara, High performance RO membranes for desalination and wastewater reclamation and their operation results, Water Sci. Technol., 62 (2010) 2134-2140.

[21] T. Sasaki, H. Tomioka, K. Nakatsuji, Composite semipermeable membrane, production process thereof, and element, fluid separation equipment and treatment method for boron-containing water using the same, in: U.S. Patent (Ed.) United States Patent, Toray Industries, Inc., USA, 2010.

[22] T. Fujioka, N. Oshima, R. Suzuki, M. Higgins, W.E. Price, R.K. Henderson, L.D. Nghiem, Effect of heat treatment on fouling resistance and the rejection of small and neutral solutes by reverse osmosis membranes, Water Sci. Technol. Water Supply, 15 (2015) 510-516.

[23] J.G. Wijmans, R.W. Baker, The solution-diffusion model: a review, J. Membr. Sci., 107 (1995) 1-21.

[24] S. Bandini, L. Bruni, 2.04 - Transport Phenomena in Nanofiltration Membranes, in: E. Drioli, L. Giorno (Eds.) Comprehensive Membrane Science and Engineering, Elsevier, Oxford, 2010, pp. 67-89.

[25] J. Wang, D.S. Dlamini, A.K. Mishra, M.T.M. Pendergast, M.C.Y. Wong, B.B. Mamba, V. Freger, A.R.D. Verliefde, E.M.V. Hoek, A critical review of transport through osmotic membranes, J. Membr. Sci., 454 (2014) 516-537.

[26] G.M. Geise, H.B. Park, A.C. Sagle, B.D. Freeman, J.E. McGrath, Water permeability and water/salt selectivity tradeoff in polymers for desalination, J. Membr. Sci., 369 (2011) 130-138.

[27] H. Ju, A.C. Sagle, B.D. Freeman, J.I. Mardel, A.J. Hill, Characterization of sodium chloride and water transport in crosslinked poly(ethylene oxide) hydrogels, J. Membr. Sci., 358 (2010) 131-141.

[28] M. Hirose, H. Ito, Y. Kamiyama, Effect of skin layer surface structures on the flux behaviour of RO membranes, J. Membr. Sci., 121 (1996) 209-215.

[29] J.R. Werber, C.O. Osuji, M. Elimelech, Materials for next-generation desalination and water purification membranes, Nature Reviews: Materials, 1 (2016) 16018.

[30] S. Karan, Z. Jiang, A.G. Livingston, Sub–10 nm polyamide nanofilms with ultrafast solvent transport for molecular separation, Science, 348 (2015) 1347-1351.

[31] L. Lin, R. Lopez, G.Z. Ramon, O. Coronell, Investigating the void structure of the polyamide active layers of thin-film composite membranes, J. Membr. Sci., 497 (2016) 365-376.

[32] M.M. Kłosowski, C.M. McGilvery, Y. Li, P. Abellan, Q. Ramasse, J.T. Cabral, A.G. Livingston, A.E. Porter, Micro-to nano-scale characterisation of polyamide structures of the SW30HR RO membrane using advanced electron microscopy and stain tracers, J. Membr. Sci., 520 (2016) 465-476.

[33] A.K. Ghosh, B.-H. Jeong, X. Huang, E.M.V. Hoek, Impacts of reaction and curing conditions on polyamide composite reverse osmosis membrane properties, J. Membr. Sci., 311 (2008) 34-45.

[34] C.Y. Tang, Y.-N. Kwon, J.O. Leckie, Characterization of humic acid fouled reverse osmosis and nanofiltration membranes by transmission electron microscopy and streaming potential measurements, Environ. Sci. Technol., 41 (2006) 942-949.

[35] V. Freger, Swelling and morphology of the skin layer of polyamide composite membranes: an atomic force microscopy study, Environ. Sci. Technol., 38 (2004) 3168-3175.

[36] F.A. Pacheco, I. Pinnau, M. Reinhard, J.O. Leckie, Characterization of isolated polyamide thin films of RO and NF membranes using novel TEM techniques, J. Membr. Sci., 358 (2010) 51-59.

[37] H. Yan, X. Miao, J. Xu, G. Pan, Y. Zhang, Y. Shi, M. Guo, Y. Liu, The porous structure of the fully-aromatic polyamide film in reverse osmosis membranes, J. Membr. Sci., 475 (2015) 504-510.

[38] Y. Li, M.M. Kłosowski, C.M. McGilvery, A.E. Porter, A.G. Livingston, J.T. Cabral, Probing flow activity in polyamide layer of reverse osmosis membrane with nanoparticle tracers, J. Membr. Sci., 534 (2017) 9-17.

[39] B. Van der Bruggen, A. Verliefde, L. Braeken, E.R. Cornelissen, K. Moons, J.Q.J.C. Verberk, H.J.C. van Dijk, G. Amy, Assessment of a semi-quantitative method for estimation of the rejection of organic compounds in aqueous solution in nanofiltration, J. Chem. Technol. Biotechnol., 81 (2006) 1166-1176.

[40] T. Fujioka, H. Takeuchi, H. Tanaka, L.D. Nghiem, K.P. Ishida, H. Kodamatani, A rapid and reliable technique for *N*-nitrosodimethylamine analysis in reclaimed water by HPLC-photochemical reaction-chemiluminescence, Chemosphere, 161 (2016) 104-111.

[41] H. Kodamatani, H. Yamasaki, T. Sakaguchi, S. Itoh, Y. Iwaya, M. Saga, K. Saito, R. Kanzaki, T. Tomiyasu, Rapid method for monitoring N-nitrosodimethylamine in drinking water at the ng/L level without pre-concentration using high-performance liquid chromatography-chemiluminescence detection, J. Chromatogr. A, 1460 (2016) 202-206.

[42] M. Eldrup, D. Lightbody, J.N. Sherwood, The temperature dependence of positron lifetimes in solid pivalic acid, Chem. Phys., 63 (1981) 51-58.

[43] S.J. Tao, Positronium annihilation in molecular substances, J. Chem. Phys., 56 (1972) 5499-5510.

[44] V. Kolev, V. Freger, Hydration, porosity and water dynamics in the polyamide layer of reverse osmosis membranes: A molecular dynamics study, Polymer, 55 (2014) 1420-1426.

[45] M. Bass, V. Freger, Facile evaluation of coating thickness on membranes using ATR-FTIR, J. Membr. Sci., 492 (2015) 348-354.

[46] E. Dražević, K. Košutić, V. Freger, Permeability and selectivity of reverse osmosis membranes: Correlation to swelling revisited, Water Res., 49 (2014) 444-452.

[47] C.Y. Tang, Y.-N. Kwon, J.O. Leckie, Effect of membrane chemistry and coating layer on physiochemical properties of thin film composite polyamide RO and NF membranes: I. FTIR and XPS characterization of polyamide and coating layer chemistry, Desalination, 242 (2009) 149-167.

[48] F. Pacheco, R. Sougrat, M. Reinhard, J.O. Leckie, I. Pinnau, 3D visualization of the internal nanostructure of polyamide thin films in RO membranes, J. Membr. Sci., 501 (2016) 33-44.

[49] J. Lee, C.M. Doherty, A.J. Hill, S.E. Kentish, Water vapor sorption and free volume in the aromatic polyamide layer of reverse osmosis membranes, J. Membr. Sci., 425–426 (2013) 217-226.

[50] E.P. Chan, A.P. Young, J.-H. Lee, J.Y. Chung, C.M. Stafford, Swelling of ultrathin crosslinked polyamide water desalination membranes, J. Polym. Sci., Part B: Polym. Phys., 51 (2013) 385-391.

[51] Y.-H. Huang, W.-C. Chao, W.-S. Hung, Q.-F. An, K.-S. Chang, S.-H. Huang, K.-L. Tung, K.-R. Lee, J.-Y. Lai, Investigation of fine-structure of polyamide thin-film composite membrane under swelling effect by positron annihilation lifetime spectroscopy and molecular dynamics simulation, J. Membr. Sci., 417–418 (2012) 201-209.

[52] E. Dražević, K. Košutić, V. Kolev, V. Freger, Does Hindered Transport Theory Apply to Desalination Membranes?, Environ. Sci. Technol., 48 (2014) 11471-11478.

[53] G.M. Geise, D.R. Paul, B.D. Freeman, Fundamental water and salt transport properties of polymeric materials, Prog. Polym. Sci., 39 (2014) 1-42.

[54] T.A. Jadwin, A.S. Hoffman, W.R. Vieth, Crosslinked poly(hydroxyethyl methacrylate) membranes for desalination by reverse osmosis, J. Appl. Polym. Sci., 14 (1970) 1339-1359.

Transport of small and neutral solutes through reverse osmosis membranes: Role of skin layer conformation of the polyamide film

Takahiro Fujioka[1,*], Brian E. O'Rourke[2], Koji Michishio[2], Yoshinori Kobayashi[2], Nagayasu Oshima[2], Hitoshi Kodamatani[3], Takuji Shintani[4], Long D. Nghiem[5]

[1]Water and Environmental Engineering, Graduate School of Engineering, Nagasaki University, 1-14 Bunkyo-machi, Nagasaki 852-8521, Japan

[2]National Metrology Institute of Japan, National Institute of Advanced Industrial Science and Technology, 1-1-1 Umezono, Tsukuba, Ibaraki 305-8568, Japan

[3]Division of Earth and Environmental Science, Graduate School of Science and Engineering, Kagoshima University, 1-21-35 Korimoto, Kagoshima 890-0065, Japan

[4]Division of Advanced Membrane Science and Technology, Graduate School of Science, Technology and Innovation, Kobe University, 1-1 Rokkodai-cho, Kobe 657-8501, Japan

[5]Strategic Water Infrastructure Laboratory, School of Civil Mining and Environmental Engineering, The University of Wollongong, NSW 2522, Australia

SUPPLEMENTARY MATERIAL

* Corresponding author: Takahiro Fujioka, Email: tfujioka@nagasaki-u.ac.jp, Ph +81 095 819 2695

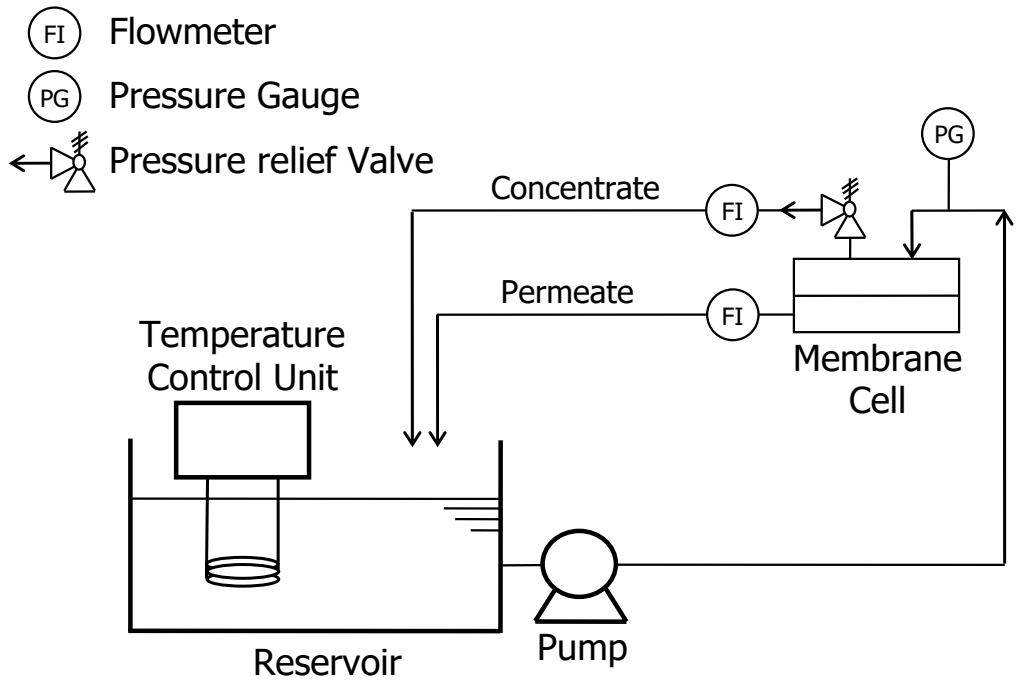

Fig. S1 – Schematic diagram of the cross-flow RO filtration system that comprised of the membrane cell, high-pressure pump (KP-12, FLOM, Tokyo, Japan), 2-L glass reservoir with a stainless steel heat exchanging coil connected to a temperature control unit (NCB-500, Tokyo Rikakikai, Tokyo, Japan). Each membrane was cut out to be fit in a circular membrane cell (Iwai Pharma Tech, Tokyo, Japan) that has an effective surface area of 36.3 cm^2.

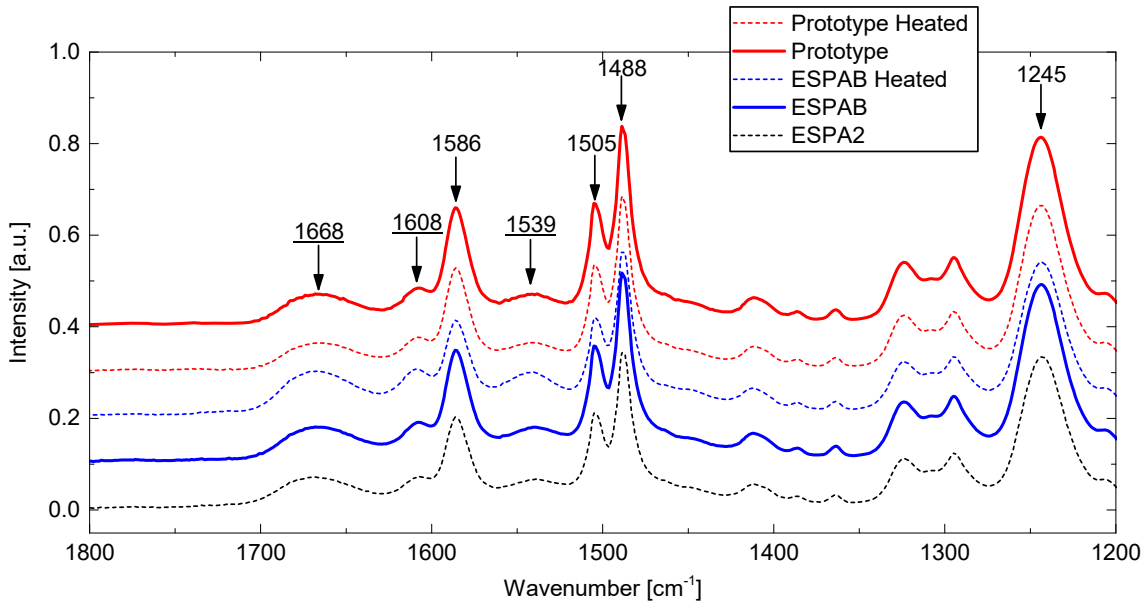

Fig. S2 – ATR-FTIR spectra for the five RO membranes. Peaks for fully aromatic polyamide are presented with underline (1668, 1608 and 1539 cm^{-1}).

Table S3 – Mean free-volume hole-radius of the selected RO membranes. The average was calculated from the data of Samples A and B.

Membrane		Average	Sample A		Sample B	
		r [nm]	r [nm]	$\tau_{o\text{-Ps}}$ [ns]	r [nm]	$\tau_{o\text{-Ps}}$ [ns]
ESPA2	untreated	0.270 ± 0.007	0.265 ± 0.007	1.787 ± 0.067	0.275 ± 0.006	1.890 ± 0.059
ESPAB	untreated	0.275 ± 0.009	0.269 ± 0.006	1.829 ± 0.059	0.281 ± 0.008	1.956 ± 0.082
	heated	0.274 ± 0.005	0.271 ± 0.005	1.842 ± 0.050	0.278 ± 0.005	1.920 ± 0.050
Prototype	untreated	0.270 ± 0.007	0.265 ± 0.004	1.781 ± 0.041	0.275 ± 0.005	1.889 ± 0.048
	heated	0.275 ± 0.012	0.284 ± 0.003	1.980 ± 0.037	0.267 ± 0.002	1.807 ± 0.024

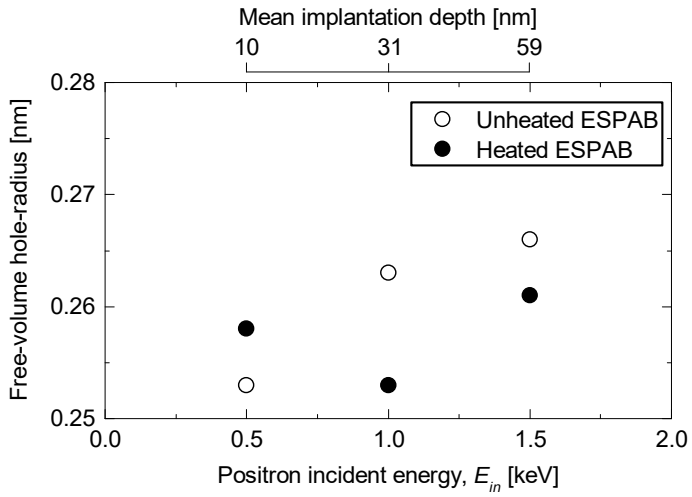

Fig. S4 – Mean free-volume hole-radius of unheated and heated ESPAB RO membranes. The ESPAB RO membrane coupons were obtained from a different sheet of those used in Table S2 and Fig. 3 and analysis was conducted in a different occasion, thus, the data presented here should be treated as reference only.

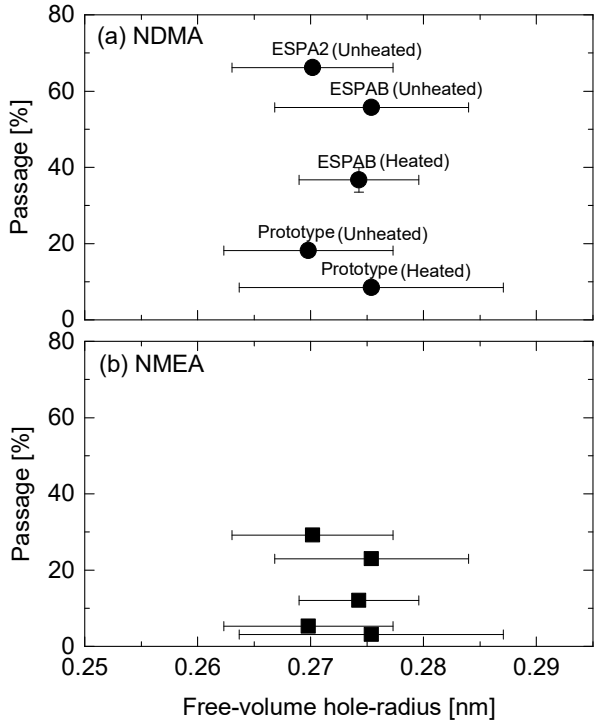

Fig. S5 – The passage of NDMA and NMEA as a function of free-volume hole-radius for the five RO membranes.

Table S6 – Average and deviation of skin layer thickness at 5 locations for each sample.

Membrane		Average [nm]	Sample A [nm]		Sample B [nm]	
			Average	Deviation	Average	Deviation
ESPA2	untreated	36 ± 4 nm	38.3	5.8	33.1	4.9
ESPAB	untreated	29 ± 3 nm	31.6	2.3	27.3	2.7
	heated	29 ± 0.2 nm	29.0	1.4	29.3	3.7
Prototype	untreated	34 ± 2 nm	35.6	6.0	32.2	5.1
	heated	31 ± 1 nm	31.5	6.1	30.4	4.9

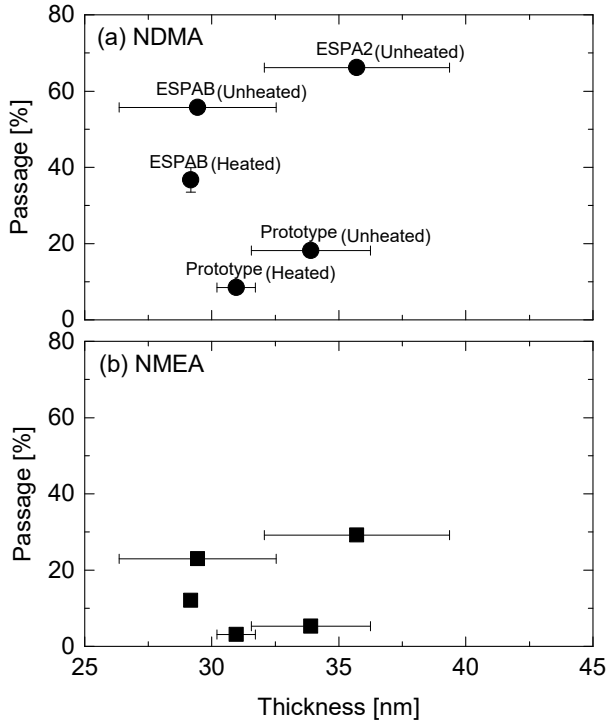

Fig. S7 – The passage of NDMA and NMEA as a function of the crumpled polyamide film thickness for the five RO membranes.